Chinese Chemical Letters 35 (2024) 108602

Contents lists available at ScienceDirect

Chinese Chemical Letters

journal homepage: www.elsevier.com/locate/cclet

Transdermal treatment for malignant melanoma by aptamer-modified tetrahedral framework nucleic acid delivery of vemurafenib

Dexuan Xiao[a,b,c], Tianyu Chen[a,b], Tianxu Zhang[a,b], Sirong Shi[a,b], Mei Zhang[a,b], Xin Qin[a,b], Yunkun Liu[a,c], Longjiang Li[a,c,*], Yunfeng Lin[a,b,*]

[a] State Key Laboratory of Oral Diseases, National Clinical Research Center for Oral Diseases, West China Hospital of Stomatology, Sichuan University, Chengdu 610041, China
[b] Sichuan Provincial Engineering Research Center of Oral Biomaterials, Chengdu 610041, China
[c] Department of Head and Neck Oncology, National Clinical Research Center for Oral Diseases, West China Hospital of Stomatology, Sichuan University, Chengdu 610041, China

ARTICLE INFO

Article history:
Received 3 April 2023
Revised 21 May 2023
Accepted 23 May 2023
Available online 28 May 2023

Keywords:
Melanoma
Vemurafenib
DNA nanostructure
Transdermal treatment
Side effect

ABSTRACT

Melanoma is one of the most malignant skin tumors, whose high invasion is generally associated with BRAF gene mutation. Although new chemotherapeutic drugs, such as vemurafenib, have been developed to inhibit the growth of melanoma, these drugs are usually administered intravenously or orally, resulting in toxic side effects on major tissues and organs. Tetrahedral framework nucleic acids (tFNAs) are a novel type of DNA nanostructures with excellent biocompatibility and versatility which have been proven to penetrate through skin barrier with ease. In this study, we prepared tFNAs with vemurafenib and connected DNA aptamer AS1411 at the apex of tFNAs (AS1411-tFNAs/vemurafenib). On one hand, AS1411-tFNAs/vemurafenib could kill melanoma cells by blocking the mutated BRAF gene *in vitro*. Compared with free vemurafenib, AS1411-tFNAs/vemurafenib had no obvious toxicity to normal cells. On the other hand, AS1411-tFNAs could transfer vemurafenib to cross through the skin barrier and permeate into tumor tissues. *In vivo*, transdermal delivery of AS1411-tFNAs/vemurafenib could inhibit the growth of human A375 melanoma, whose inhibiting effect was stronger than intravenous administration of vemurafenib. These results demonstrated the application prospects of tFNAs combined with chemotherapeutic drugs in skin tumors.

Melanoma originates from melanocytes, and it is one of the most lethal skin tumors all over the world, because of its aggressive metastasis and high recurrence [1,2]. To date, there were approximately 300,000 new melanoma patients each year, and the morbidity is still rapidly increasing [3,4]. Early-stage melanoma is usually curable with timely surgical intervention. Patients with advanced melanoma are mainly treated with radiotherapy, chemotherapy, and immunotherapy to inhibit tumor growth. However, due to drug resistance or immune tolerance, it often leads to poor prognosis [5,6]. Furthermore, these therapies tend to damage healthy organs and cause great toxic side effects for poor tissue selectivity [7]. Given the existence of mutant genes that greatly stimulate the growth of melanoma, scientists work on novel chemotherapy agents, such as dabrafenib, trametinib and nivolumab, to target and inhibit these genes, resulting in enhanced therapeutic efficacy, reduced toxicity, and prolonged median survival time [8,9]. BRAF gene plays a key role in mitogen-activated protein kinase (MAPK) signaling pathway, and BRAF gene mutation is reported to occur in most melanomas, which accelerates tumor development and metastasis [10–12]. Vemurafenib is a kind of small molecule inhibitors of BRAF V600E (the most common BRAF mutation) and can significantly improve the progression-free survival of advanced melanoma patients [13,14]. However, due to oral or intravenous administration, vemurafenib might cause renal or hepatic impairment [15,16]. Thus, considering melanomas are mainly subcutaneous, transdermal vemurafenib delivery has good prospects.

To achieve the transdermal delivery of drugs, various attempts were performed, such as electroporation, microneedle, and modification of chemical compounds, but these approaches probably infect or injure the skin [17–19]. In the past several years, transdermal carriers have been designed to enhance the skin penetration of drugs, which can improve the convenience of treatment with no invasion [20–23]. DNA nanotechnology employs complemen-

* Corresponding authors.
E-mail addresses: muzili63@163.com (L. Li), yunfenglin@scu.edu.cn (Y. Lin).

https://doi.org/10.1016/j.cclet.2023.108602
1001-8417/

tary pairing of DNA single strands to form specific spatial structures [24]. Compared with other conventional nanostructures, DNA nanomaterials have structural diversity, remarkable editability, and biocompatibility [25,26]. Tetrahedral framework nucleic acids (tFNAs) stand out from the crowd of DNA nanostructures by their simple synthesis, low cost, and high yield [27–29]. tFNAs penetrate through the cell membrane with ease and possess multiple modification sites for small molecules, aptamers, or RNA agents, which make tFNAs widely used in drug delivery, gene therapy, and biosensor [30–32]. In addition, it was reported that tFNAs could cross through the skin barrier and permeate into the subcutaneous tissues [33,34]. Given all this, tFNAs are expected to be good transdermal drug delivery systems for various skin diseases.

In this study, we fabricated tFNAs with vemurafenib for transdermal therapy of skin malignant melanoma. To enhance the targeting and therapeutic efficacy of our transdermal carrier, we modified a DNA aptamer AS1411, which shows a high affinity for nucleolin expressed on the membrane of multiple tumor cells, at the vertex of tFNAs. Compared with vemurafenib, AS1411-tFNAs/vemurafenib could penetrate through the skin and kill melanoma cells without systemic effects. The combination of small molecules, DNA nanostructures, and nucleic acid aptamers may provide a new method for the transdermal treatment of skin tumors.

The tFNAs were prepared according to previous studies [35–37]. Four designed single-strand DNA (ssDNA) strands were self-assembled with an equivalent molar ratio in TM buffer (10 mmol/L Tris-HCl, 50 mmol/L $MgCl_2$, pH 8.0). The tFNAs were synthesized after heating to 95 °C for 10 min and annealing to 4 °C for 20 min. Next, the sequence of aptamer AS1411 was added to S4, and the AS1411-tFNAs were synthesized as the aforementioned procedure by replacing S4 with S4-AS1411. All the ssDNA sequences were listed in Table S1 (Supporting information). The vemurafenib powder was dissolved in dimethyl sulfoxide (DMSO), then mixed with tFNAs or AS1411-tFNAs at different ratios and shaken for 6 h at room temperature. The products were purified to remove free vemurafenib by Millipore Amicon Ultra (30 kDa, 500 μL, USA).

Polyacrylamide gel electrophoresis (PAGE) was applied to verify the synthesis of tFNAs, AS1411-tFNAs, and AS1411-tFNAs/vemurafenib. The zeta potential and size of AS1411-tFNAs and AS1411-tFNAs/vemurafenib were detected by dynamic light scattering (DLS, Nano ZS, Malvern, UK). Meanwhile, the morphology information was obtained *via* atomic force microscopy (AFM, SPM 9700, Shimadzu, Japan). For the further detection that vemurafenib was loaded into AS1411-tFNAs, the ultraviolet (UV) absorbances of AS1411-tFNAs, vemurafenib, and AS1411-tFNAs/vemurafenib were recorded *via* UV spectrophotometer (Nanophotometer N60, Implen, Germany) at 318 nm. The loading ratio of vemurafenib and AS1411-tFNAs was calculated as follows: Loading ratio = (Loading vemurafenib)/(Total AS1411-tFNAs).

Detailed materials and methods of cellular experiments could be found in Supporting information.

The mice experiments were approved by the Ethics Committee of West China Hospital of Stomatology (Approval Number: WCHSIRB-D-2021-222) and performed according to the relevant laws and institutional guidelines. Female BALB/c nude mice of 3–4 weeks were raised in specific pathogen free (SPF) environment and divided into six groups (4 mice per group), including control group, tFNAs group, tFNAs/vemurafenib group, AS1411-tFNAs/vemurafenib group, vemurafenib (transdermal) group, and vemurafenib (intravenous) group. To establish malignant melanoma modes, 1×10^6 A375 cells in 100 μL DMEM medium were injected subcutaneously into the left armpit. When tumors grew to ~100 mm^3, prepared drugs were mixed with Aquaphor (Eucerin, Germany) and wiped evenly on the surface of the tumors with surgical dressing (Tegaderm, 3M, USA) covered. In Group 6, vemurafenib (250 μmol/L, 100 μL) was injected intravenously. Each group of mice was handled daily with related drugs, and tumor volume and mouse weight were measured once every two days. Tumor volume was calculated by $W^2 \times L \times 0.5$, in which W referred to the shortest diameter of tumor and L referred to the longest diameter. After 10 doses, mice were sacrificed and harvested for tumors and organs (skin, liver, heart, lung, kidney, and spleen). All tissues were fixed in paraformaldehyde and subjected to hematoxylin-eosin (H&E) staining. Besides, tumor sections were stained for immunofluorescence detection.

C57/BL mice were divided into four groups, which included tFNAs group, tFNAs/vemurafenib group, AS1411-tFNAs/vemurafenib group, and control group. In this section, tFNAs were labeled with Cy5 fluorescence. C57 mice were removed the hair on the back in advance. Cy5-labeled samples were mixed with Aquaphor and smeared evenly on the hairless area of the mice. Then, the treated back was covered with a surgical dressing. After penetration for 24 h, the treated skin was cleaned and collected for frozen sections. To detect the penetration of drugs in A375 tumor, tumor-bearing BALB/c nude mice were handled with Cy5-labeled agents as the same methods above. The tumors were also collected for fluorescence detection.

All results were presented as mean ± standard deviation (SD). One-way ANOVA and *t*-test were applied for statistical analysis in GraphPad Prism 7.0 (GraphPad Software Inc., USA). When P was less than 0.05, the results were considered statistically significant.

A simplified synthesis procedure is shown in Fig. 1A. Four designed ssDNA strands (S1, S2, S3 and S4) were self-assembled into tFNAs in TM buffer by complementary pairing [38,39]. Then we connected the aptamer AS1411 sequence to 5′ end of S4, and synthesized AS1411-tFNAs as the same procedure above. All ssDNA sequences were exhibited in Table S1. The fabrication of tFNAs and AS1411-tFNAs was detected by 8% PAGE (Fig. 1B). The band of tFNAs moved faster than that of AS1411-tFNAs in PAGE, implying the synthesis of AS1411-tFNAs.

Next, we mixed different concentrations of vemurafenib (5, 10, 20, and 50 μmol/L) with AS1411-tFNAs (1 μmol/L) and shook the samples at room temperature for 6 h. Considering the positive charge of vemurafenib, vemurafenib might be adsorbed onto tFNAs through electrostatic interaction (Fig. S1A in Supporting information). PAGE was also applied to verify the combination of vemurafenib and AS1411-tFNAs (Fig. 1C). With the increasing concentration of vemurafenib, the migration rate of bands was getting lower, demonstrating the rising loading amount of vemurafenib on AS1411-tFNAs. To further monitor the maximum loading capacity, we removed residual vemurafenib by ultrafiltration and detected it with an ultraviolet spectrophotometer (Fig. 1D). It was obvious that the peak of AS1411-tFNAs/vemurafenib was high than that of AS1411-tFNAs at the same concentration. Moreover, according to the standard curve of vemurafenib, the maximum loading ratio of vemurafenib and AS1411-tFNAs was about 25:1 (Fig. S1B in Supporting information).

To observe the morphology of our nanostructures, AFM was employed, and the results illustrated that the size of AS1411-tFNAs/vemurafenib was slightly larger than AS1411-tFNAs (Figs. 1E and F). Meanwhile, AS1411-tFNAs/vemurafenib still maintained a tetrahedral-like spatial structure. The excellent tissue penetration of tFNAs owes much to such a three-dimension structure [34,40]. Next, we further detected the size and shape of AS1411-tFNAs and AS1411-tFNAs/vemurafenib *via* transmission electron microscope (TEM). As shown in Fig. S2 (Supporting information), the images of TEM indicated the growing in size and change in morphology of AS1411-tFNAs/vemurafenib, which was consistent with AFM and further demonstrated the successful synthesis of AS1411-tFNAs/vemurafenib. Finally, we utilized DLS to detect the particle size and zeta potential of AS1411-tFNAs and AS1411-

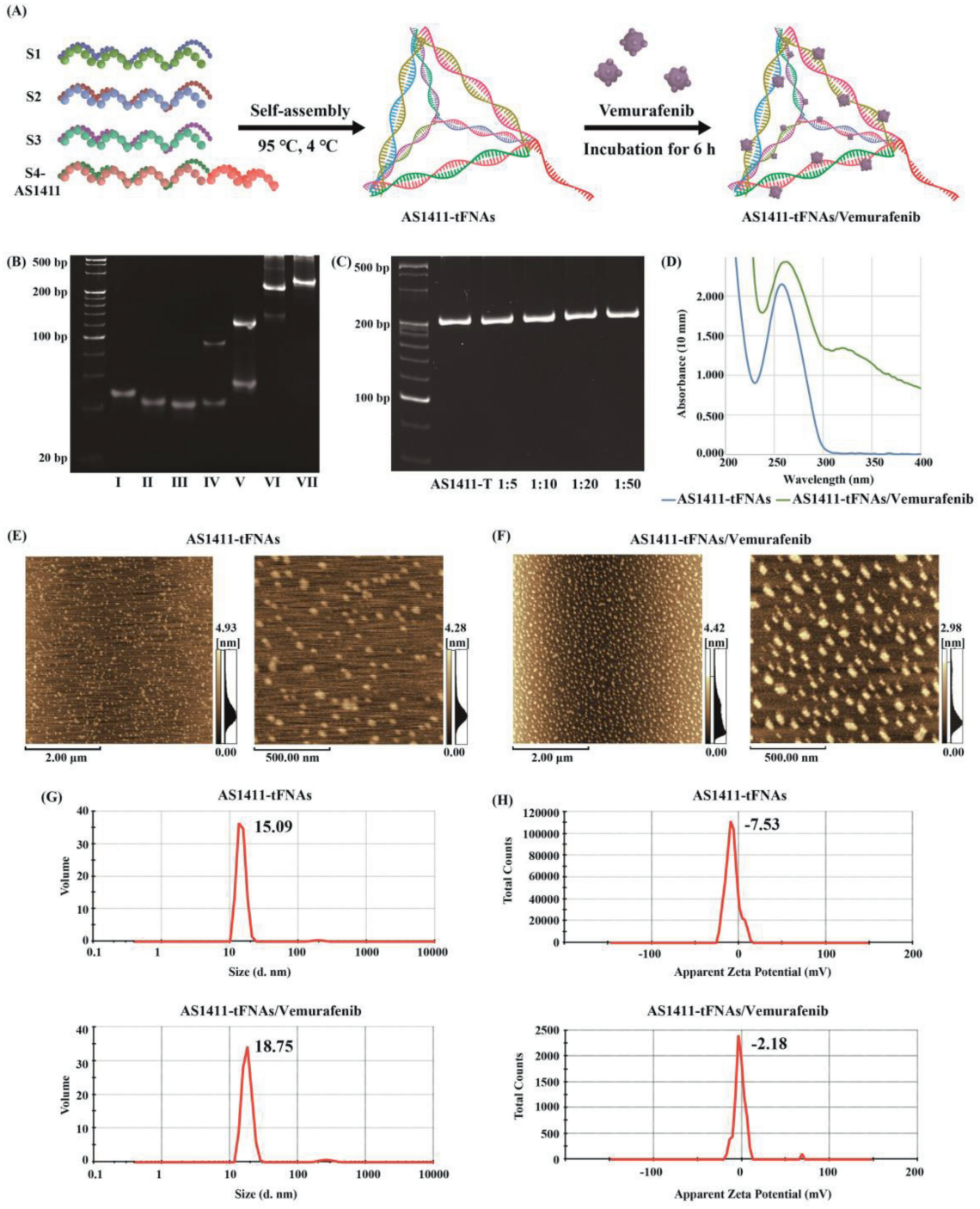

Fig. 1. Successful synthesis and characterization of AS1411-tFNAs/vemurafenib. (A) Schematic diagram showing the composition of AS1411-tFNAs and AS1411-tFNAs/vemurafenib. (B) PAGE graph showing the synthesis of AS1411-tFNAs (I: S1, II: S2, III: S3, IV: S4, V: S4-AS1411, VI: tFNAs, VII: AS1411-tFNAs). (C) PAGE graph analysis of AS1411-tFNAs/vemurafenib with different AS1411-tFNAs: Vemurafenib ratios (AS1411-T refers to AS1411-tFNAs). (D) UV absorption spectroscopy of AS1411-tFNAs and AS1411-tFNAs/vemurafenib. (E, F) AFM images of AS1411-tFNAs and AS1411-tFNAs/vemurafenib, respectively. Scale bars are 2 μm and 500 nm. (G) Hydrodynamic sizes of AS1411-tFNAs and AS1411-tFNAs/vemurafenib measured by DLS. (H) Zeta potentials of AS1411-tFNAs and AS1411-tFNAs/vemurafenib.

tFNAs/vemurafenib (Figs. 1G and H). The particle size of AS1411-tFNAs was 15.09 nm, and AS1411-tFNAs/vemurafenib's was a little larger (18.75 nm), which accorded with the results of AFM. Meanwhile, the zeta potential of AS1411-tFNAs (−7.53 mV) was more negative than that of AS1411-tFNAs/vemurafenib (−2.18 mV). All of the above results verified the successful synthesis of AS1411-tFNAs/vemurafenib.

To measure the uptake of AS1411-tFNAs/vemurafenib by A375 cells, S1 strand was modified with Cy5 fluorescein to form Cy5-AS1411-tFNAs/vemurafenib as the same procedure mentioned above. After being treated with the related samples for 12 h, we conducted a confocal microscope to detect the cellular uptake. As shown in Fig. 2A, the fluorescence intensity of tFNAs/vemurafenib was weaker than pure tFNAs, but the fluorescence intensity of AS1411-tFNAs/vemurafenib was almost as strong as that of tFNAs. The results indicated that tFNAs could transfer vemurafenib into A375 cells, and aptamer AS1411 further enhanced the cellular internalization of our carriers due to its affinity with nucleolin ex-

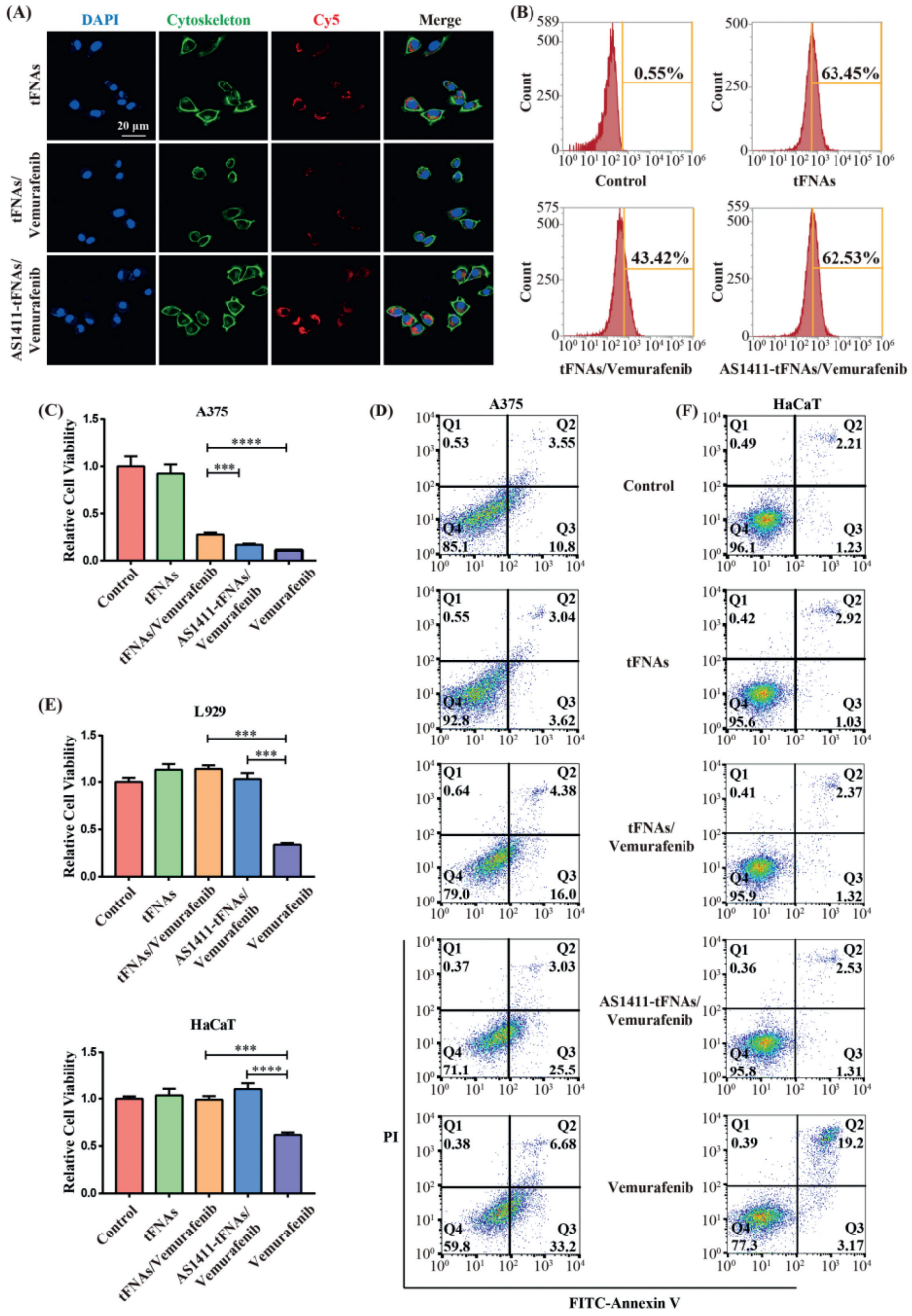

Fig. 2. Cellular uptake of AS1411-tFNAs/vemurafenib and cell viability. (A) Cellular uptake of tFNAs, tFNAs/vemurafenib or AS1411-tFNAs/vemurafenib in A375 cells detected by confocal laser microscope (nucleus: blue; cytoskeleton: green; Cy5: red). Scale bars are 20 μm. (B) Flow cytometry analysis of the proportion of A375 cells uptake of tFNAs, tFNAs/vemurafenib or AS1411-tFNAs/vemurafenib. (C) CCK-8 assays to detect the inhibitory effect of AS1411-tFNAs/vemurafenib on A375 cells ($n = 5$). (D) Cell apoptosis analysis of A375 cells by flow cytometry. (E) CCK-8 assays to detect the side toxic effect of AS1411-tFNAs/vemurafenib on L929 and HaCaT cells ($n = 5$). (F) Cell apoptosis analysis of HaCaT cells by flow cytometry. Data are presented as mean ± SD. Statistical analysis: $^{***}P < 0.001$, $^{****}P < 0.0001$.

pressed in A375 cells [41,42]. In addition, flow cytometry was utilized to detect cellular uptake (Fig. 2B). The uptake level of AS1411-tFNAs/vemurafenib (62.53%) was significantly stronger than that of tFNAs/vemurafenib (43.42%), and the results were consistent with fluorescence detection.

The concentration of tFNAs was investigated *via* CCK-8 assay, and its result indicated that 62.5 nmol/L or 125 nmol/L tFNAs showed less influence on the cell viability of A375 cells (Fig. S3 in Supporting information). Furthermore, 125 nmol/L tFNAs could protect multiple epithelial and mesenchymal cells from damage factors according to previous reports [36,43]. Therefore, 125 nmol/L tFNAs were applied in the subsequent experiments. Next, the inhibiting effects of AS1411-tFNAs/vemurafenib on the growth of A375 cells were detected *via* CCK-8 and cell apoptosis assay (Figs. 2C and D). Both results indicated that AS1411-tFNAs/vemurafenib had a stronger inhibiting effect on A375 cell viability than tFNAs/vemurafenib, and this might be caused by increased cellular uptake of AS1411-tFNAs/vemurafenib.

In addition, we evaluated the cytotoxicity of AS1411-tFNAs/vemurafenib to normal cells through the two methods mentioned above. L929 and HaCaT cells took the same treatment as A375 cells. As shown in Fig. 2E, neither tFNAs/vemurafenib nor AS1411-tFNAs/vemurafenib were cytotoxic to L929 and HaCaT cells, while simplex vemurafenib had obvious cytotoxicity.

The result of cell apoptosis detection was consistent with the CCK-8 assay (Fig. 2F). Free vemurafenib could induce HaCaT cell apoptosis, but failed induction in tFNAs/vemurafenib and AS1411-tFNAs/vemurafenib. In theory, vemurafenib only inhibits the growth of cells with BRAF gene mutation. However, previous studies reported that vemurafenib was easily encapsulated in cell membranes due to its hydrophobic property and caused damage to membranes without cell specificity [44]. tFNAs could transfer vemurafenib into cells but avoid cell membrane damage, resulting in inapparent toxic effects on normal cells. Furthermore, those results implied that the poor hydrophobicity of vemurafenib might contribute to its slightly stronger inhibition on the growth of A375 cells compared with AS1411-tFNAs/vemurafenib, and tFNAs might not weaken the tumor-killing effect of vemurafenib.

The variation of apoptosis proteins was another aspect to evaluate the killing effect of AS1411-tFNAs/vemurafenib on A375 cells. The expression of caspase-3, Bcl-2 and Bax was detected by Western blot (Figs. S4D and E in Supporting information). After being treated with AS1411-tFNAs/vemurafenib, the expression of caspase-3 and Bax both increased and the expression of Bcl-2 decreased. Meanwhile, the variation of apoptosis proteins in AS1411-tFNAs/vemurafenib group was more conspicuous than tFNAs/vemurafenib group. Considering the key role of caspase-3 in apoptosis pathway, we also observed its expression by im-

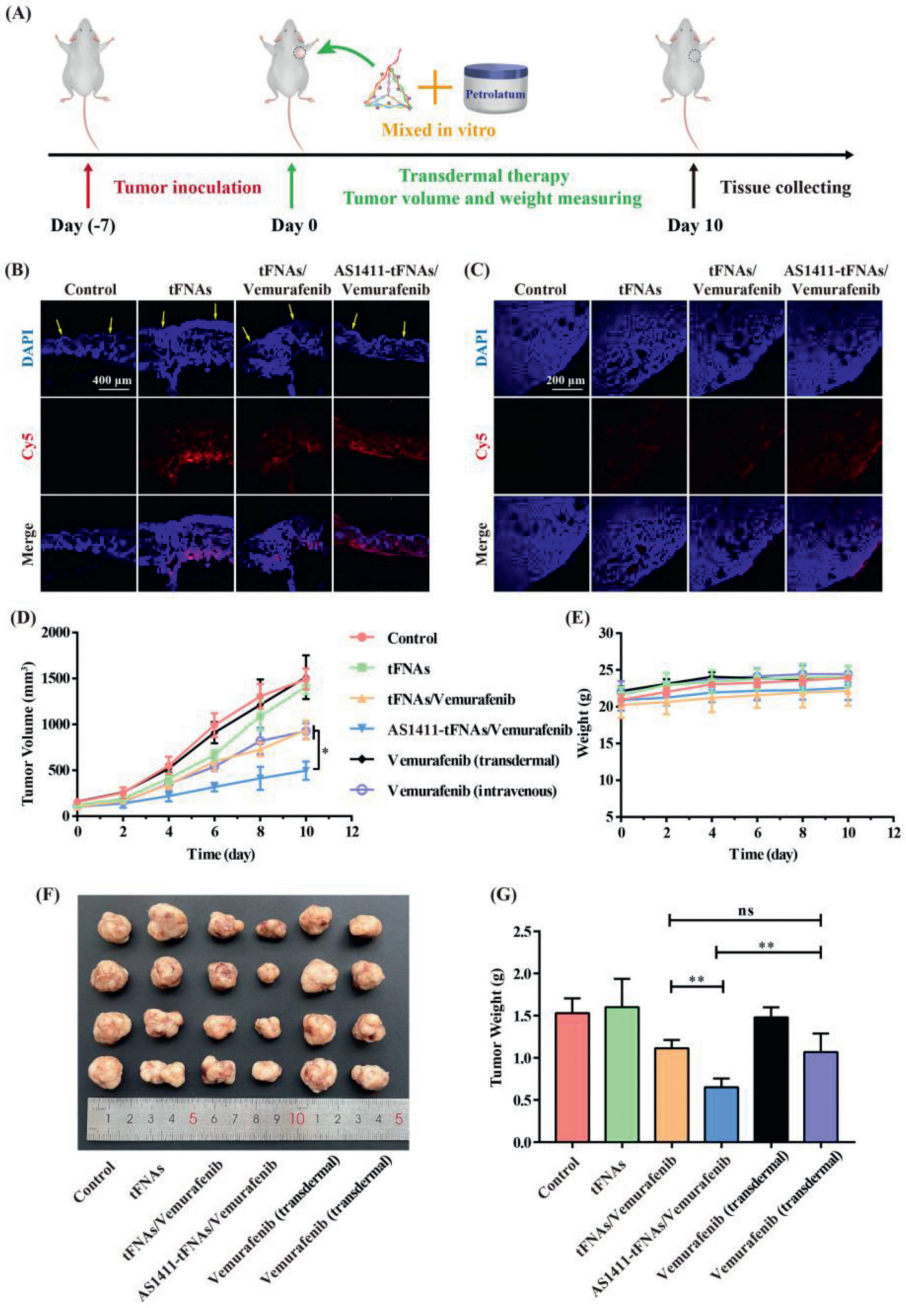

Fig. 3. Transdermal test and antitumor evaluation of AS1411-tFNAs/vemurafenib *in vivo*. (A) Schematic illustration of the transdermal therapy of subcutaneous melanoma. (B, C) Fluorescence imaging of skin and tumor histological sections following tFNAs, tFNAs/vemurafenib or AS1411-tFNAs/vemurafenib transdermal application (nucleus: blue; Cy5: red; stratum corneum: yellow arrow). Scale bars are 400 and 200 μm. (D) Tumor growth curves of tumor-bearing mice received various treatments ($n = 4$). (E) Body weight recorded in the experiment ($n = 4$). (F) Tumors excised from tumor-bearing mice after 10 days. (G) Comparison of tumor weight ($n = 4$). Data are presented as mean ± SD. Statistical analysis: $^{*}P < 0.05$, $^{**}P < 0.01$ (ns: no significance).

munofluorescence detection (Fig. S4A in Supporting information). The result illustrated that the fluorescence intensity of caspase-3 in AS1411-tFNAs/vemurafenib group was boosted and stronger than tFNAs/vemurafenib group, which was consistent with Western blot.

Next, to verify the influence of AS1411-tFNAs on the mechanism of vemurafenib, Western blot and immunofluorescence detection were also used to measure the expression of BRAF kinase (Figs. S4B, F, and G in Supporting information). Similar to free vemurafenib at equal concentration, AS1411-tFNAs/vemurafenib could downregulate the expression of BRAF, and the downregulation effect was stronger than tFNAs/vemurafenib. Moreover, the mutant BRAF in melanoma can unconventionally activate the level of phosphorylated extracellular regulated protein kinases (ERK) in MAPK signaling pathway, which is not influenced by upstream RAS kinase [45,46]. The high phosphorylation of ERK contributes to cell proliferation, DNA damage repair, and prevention of cell apoptosis. As shown in Figs. S4C, F, and G (Supporting information), af-

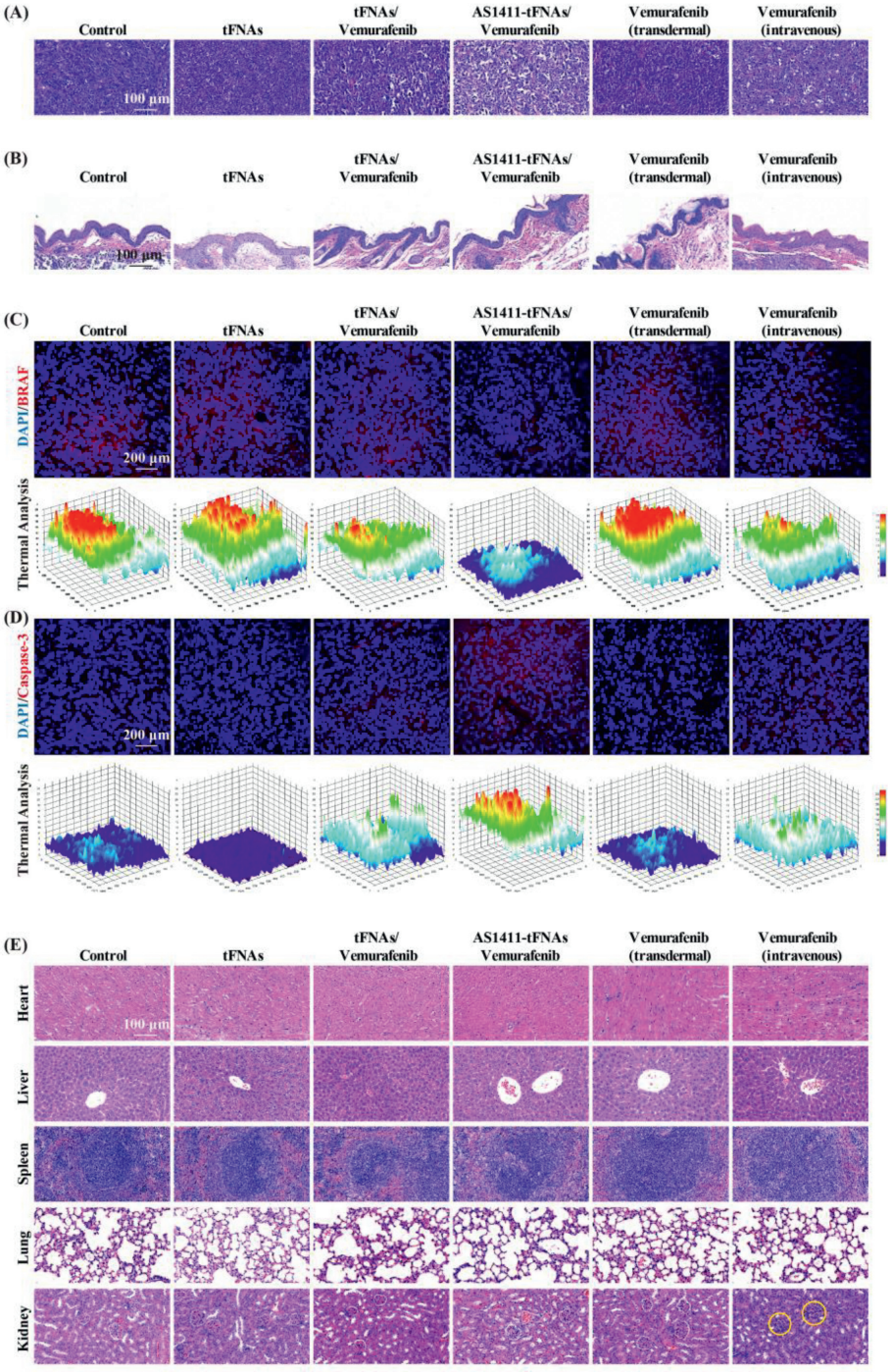

Fig. 4. Histopathological analysis of tumors, skins, and other important organs. (A, B) H&E staining of excised tumors and skins covered on subcutaneous tumors in different treatment groups. Scale bars are 100 μm. (C, D) Immunofluorescence micrographs of tumor tissues (nucleus: blue; BRAF, caspase-3: red). Scale bars are 200 μm. (E) H&E staining of harvested heart, liver, spleen, lung, and kidney after different treatment for 10 days (yellow circle: atrophy of glomerular basement membrane). Scale bars are 100 μm.

ter being treated with AS1411-tFNAs/vemurafenib, the phosphorylated level of ERK was decreased and consistent with the variation tendency of BRAF kinase. Meanwhile, these results further demonstrated the mechanism of cell apoptosis induced by AS1411-tFNAs/vemurafenib.

To evaluate the transdermal ability of AS1411-tFNAs/vemurafenib, we mixed saline and Cy5-labeled drugs with Aquaphor and smeared them on the back of C57 mice that were already depilated. Then, Tegaderm was applied to protect the treated area. After penetration for 24 h, we wiped off the residual Aquaphor and collected the treated back skin for frozen sections (Fig. 3B). Like simplex tFNAs, AS1411-tFNAs/vemurafenib showed strong red fluorescence at the basal layer of skin. The result implied that the modification of AS1411 and vemurafenib could not significantly disturb the transdermal ability of tFNAs. Furthermore, it has been reported that linear DNA nanomaterials are weak in skin penetration [47].

Next, to explore the permeation ability of AS1411-tFNAs/vemurafenib after crossing through the skin barrier, we conducted the same drug administration as mentioned above on A375 tumor mice. After being treated for 24 h, tumors were separated and washed for frozen sections (Fig. 3C). The fluorescence images illustrated that all of the three Cy5 labeled agents could reach 300–400 μm depth from the surface of tumor. Moreover, the fluorescence intensity of AS1411-tFNAs/vemurafenib was stronger than tFNAs or tFNAs/vemurafenib, which was attributable to enhanced target and uptake of AS1411-tFNAs/vemurafenib by melanoma cells.

The *in vivo* antitumor ability of AS1411-tFNAs/vemurafenib was detected on BALB/c nude mice, and a schematic diagram of the modeling and treatment procedure is shown in Fig. 3A. The synthesized drugs (1 μmol/L of tFNAs, tFNAs/vemurafenib, AS1411-tFNAs/vemurafenib) and 25 μmol/L of vemurafenib were mixed with Aquaphor and then applied on the tumors. In addition, vemurafenib (250 μmol/L) was administered by caudal vein. These treatments were performed every day, and tumor volume and mice weight were measured every two days. As shown in Fig. 3D, AS1411-tFNAs/vemurafenib inhibited the growth of melanoma tumors, and its antitumor efficiency was higher than intravenous administration of vemurafenib. In addition, there was no significant difference between the groups that received transdermal treatment of tFNAs or vemurafenib and the control group. After 10 days of treatment, excised tumor photograph and tumor weight further indicated that AS1411-tFNAs/vemurafenib had the strongest inhibition on the growth of melanoma tumors among all experimental groups (Figs. 3F and G).

Tumors and important organs of mice were collected for histopathological examination and immunofluorescence staining. As shown in Fig. 4A, the H&E staining results illustrated that tumor cell death and atrophy in cell shape and size were most obvious to observe after being treated with AS1411-tFNAs/vemurafenib. Furthermore, the fluorescence intensity of BRAF in AS1411-tFNAs/vemurafenib group was the weakest, while the fluorescence intensity of caspase-3 was the strongest (Figs. 4C and D). The findings demonstrated that AS1411-tFNAs/vemurafenib could downregulate the expression of BRAF kinase and induce tumor cell death. Meanwhile, the weight of mice was not significantly decreased, and the H&E staining of skin and other important organs did not display inflammation and pathological injury, which indicated the good biocompatibility and biosafety of AS1411-tFNAs/vemurafenib *in vivo* (Fig. 3E and Figs. 4B and E). In contrast, the thinning of skin thickness could be observed after transdermal administration of vemurafenib, while atrophy of glomerular basement membrane (yellow circles in Fig. 4E) was detected in vemurafenib intravenous injection group. These results further demonstrated the superiority of transdermal delivery and target therapy with AS1411-tFNAs/vemurafenib.

In this study, we demonstrated the transdermal therapeutic effect of AS1411-tFNAs/vemurafenib on subcutaneous malignant melanoma. By simple procedures, we combined tFNAs with two types of antitumor drugs, DNA aptamer AS1411 and BRAF inhibitor vemurafenib. AS1411-tFNAs/vemurafenib could inhibit the growth of A375 melanoma cells through downregulating the expression of mutant BRAF kinase and inducing cell apoptosis. Meanwhile, AS1411-tFNAs/vemurafenib showed no cytotoxicity to normal epithelial and mesenchymal cells, which might be caused by reducing supererogatory damage of vemurafenib to cell membrane. Similar to tFNAs, AS1411-tFNAs/vemurafenib could penetrate through the skin barrier and permeate into the subcutaneous tumor. Furthermore, considering the targeting of AS1411 to nucleolin, AS1411-tFNAs/vemurafenib was more readily taken up by melanoma cells. In tumor-bearing mice, transdermal treatment with AS1411-tFNAs/vemurafenib showed stronger antitumor efficiency compared with transdermal and intravenous administration of vemurafenib. Throughout the treatment process, AS1411-tFNAs/vemurafenib had no significant toxic side effects, which indicated the good biocompatibility of our DNA nanomaterials. In summary, versatile DNA nanostructures based on tFNAs are promising in transdermal drug delivery. Our combination of multiple antitumor agents and tFNAs may provide a new therapeutic strategy for subcutaneous tumor *via* the percutaneous route.

Declaration of competing interest

The authors declare that they have no known competing financial interests or personal relationships that could have appeared to influence the work reported in this paper.

Acknowledgments

This work was supported by National Key R&D Program of China (No. 2019YFA0110600), National Natural Science Foundation of China (No. 81970916), Sichuan Science and Technology Program (No. 2022NSFSC0002), Sichuan Province Youth Science and Technology Innovation Team (No. 2022JDTD0021), Research and Develop Program, West China Hospital of Stomatology Sichuan University (No. RD03202302). The authors would like to thank Liying Hao (State Key Laboratory of Oral Diseases, West China Hospital of Stomatology, Sichuan University) for the help in characterizing with AFM.

Supplementary materials

Supplementary material associated with this article can be found, in the online version, at doi:10.1016/j.cclet.2023.108602.

References

[1] D. Schadendorf, D.E. Fisher, C. Garbe, et al., Nat. Rev. Dis. Primers 1 (2015) 15003.
[2] P. Dietrich, S. Kuphal, T. Spruss, et al., Oncogene 37 (2018) 897–911.
[3] H. Sung, J. Ferlay, R.L. Siegel, et al., CA Cancer J. Clin. 71 (2021) 209–249.
[4] A. Jemal, S.S. Devesa, P. Hartge, et al., J. Natl. Cancer Inst. 93 (2001) 678–683.
[5] C.M. Balch, J.E. Gershenwald, S.J. Soong, et al., J. Clin. Oncol. 27 (2009) 6199–6206.
[6] S. Carr, C. Smith, J. Wernberg, Surg. Clin. North. Am. 100 (2020) 1–12.
[7] M.B. Atkins, J. Hsu, S. Lee, et al., J. Clin. Oncol. 26 (2008) 5748–5754.
[8] L. Finn, S.N. Markovic, R.W. Joseph, BMC Med. 10 (2012) 23.
[9] K.T. Flaherty, F.S. Hodi, B.C. Bastian, Curr. Opin. Oncol. 22 (2010) 178–183.
[10] H. Davies, G.R. Bignell, C. Cox, et al., Nature 417 (2002) 949–954.
[11] M. Colombino, M. Capone, A. Lissia, et al., J. Clin. Oncol. 30 (2012) 2522–2529.
[12] A. De Luca, M.R. Maiello, A. D'alessio, et al., Expert Opin. Ther. Targets 16 Suppl. 2 (2012) S17–S27.
[13] J.A. Sosman, K.B. Kim, L. Schuchter, et al., N. Engl. J. Med. 366 (2012) 707–714.
[14] P.B. Chapman, A. Hauschild, C. Robert, et al., N. Engl. J. Med. 364 (2011) 2507–2516.
[15] E.K. Spengler, D.E. Kleiner, R.J. Fontana, Hepatology 65 (2017) 745–748.

[16] V. Launay-Vacher, S. Zimner-Rapuch, N. Poulalhon, et al., Cancer 120 (2014) 2158–2163.
[17] D.S. Bernardi, C. Bitencourt, D.S.C. Da Silveira, et al., Nanomedicine 12 (2016) 2439–2448.
[18] R. Ruan, P. Jin, L. Zhang, et al., Mol. Pharm. 11 (2014) 4015–4022.
[19] Y. Chen, Y. Shen, X. Guo, et al., Nat. Biotechnol. 24 (2006) 455–460.
[20] A. Alexander, S. Dwivedi, Ajazuddin, et al., J. Control. Release 164 (2012) 26–40.
[21] A.Z. Alkilani, M.T.C. Mccrudden, R.F. Donnelly, Pharmaceutics 7 (2015) 438–470.
[22] V.K. Rai, N. Mishra, K.S. Yadav, et al., J. Control. Release 270 (2018) 203–225.
[23] M.R. Prausnitz, R. Langer, Nat. Biotechnol. 26 (2008) 1261–1268.
[24] P.W.K. Rothemund, Nature 440 (2006) 297–302.
[25] T. Tian, T. Zhang, S. Shi, et al., Nat. Protoc. 18 (2023) 1028–1055.
[26] T. Tian, Y. Li, Y. Lin, Bone Res. 10 (2022) 40.
[27] J. Li, Y. Yao, Y. Wang, et al., Adv. Mater. 34 (2022) e2202513.
[28] Z. Liu, X. Chen, W. Ma, et al., Adv. Funct. Mater. 32 (2022) 2204587.
[29] Y. Wen, M. Zhang, Y. Yao, et al., Chin. Chem. Lett. 34 (2023) 107549.
[30] Y. Gao, X. Chen, T. Tian, et al., Adv. Mater. 34 (2022) e2201731.
[31] T. Zhang, H. Ma, X. Zhang, et al., Adv. Funct. Mater. 33 (2023) 2213401.
[32] B. Zhang, T. Tian, D. Xiao, et al., Adv. Funct. Mater. 32 (2022) 2109728.
[33] S. Li, Y. Liu, T. Zhang, et al., Adv. Mater. 34 (2022) e2204287.
[34] C. Wiraja, Y. Zhu, D.C.S. Lio, et al., Nat. Commun. 10 (2019) 1147.
[35] R. Yan, W. Cui, W. Ma, et al., ACS Nano 17 (2023) 8767–8781.
[36] M. Zhang, Y. Wen, Z. Huang, et al., Chem. Eng. J. 435 (2023) 134855.
[37] Y. Wang, W. Jia, J. Zhu, R. Xu, Y. Lin, Chin. Chem. Lett. 34 (2023) 107746.
[38] X. Qin, L. Xiao, N. Li, et al., Bioact. Mater. 14 (2022) 134–144.
[39] W. Ma, Y. Yang, J. Zhu, et al., Adv. Mater. 34 (2022) e2109609.
[40] L. Liang, J. Li, Q. Li, et al., Angew. Chem. Int. Ed. 53 (2014) 7745–7750.
[41] D. Xiao, Y. Li, T. Tian, et al., ACS Appl. Mater. Interfaces 13 (2021) 6109–6118.
[42] L. Li, J. Hou, X. Liu, et al., Biomaterials 35 (2014) 3840–3850.
[43] J.Y. Zhu, M. Zhang, Y. Gao, et al., Signal. Transduct. Target. Ther. 5 (2020) 120.
[44] M. Peacock, R. Brem, P. Macpherson, et al., Nucleic Acids Res. 42 (2014) 13714–13722.
[45] H. Rajagopalan, A. Bardelli, C. Lengauer, et al., Nature 418 (2002) 934.
[46] E.W. Joseph, C.A. Pratilas, P.I. Poulikakos, et al., Proc. Natl. Acad. Sci. U. S. A. 107 (2010) 14903–14908.
[47] F. Shen, L. Sun, L. Wang, et al., Nano Lett. 22 (2022) 4509–4518.